Disentangling the Peak and Background Signals in Surface-Enhanced Raman Scattering

James T. Hugall, Jeremy J. Baumberg,* and Sumeet Mahajan*

NanoPhotonics Centre, Cavendish Laboratory, University of Cambridge, CB3 0HE, United Kingdom

ABSTRACT: Understanding the complex relationship between peak enhancement and the underlying broad continuum (called the "background") is crucial for developing reliable and quantitative applications of surface-enhanced Raman scattering (SERS). Here we use a gentle mechanochemical ("snow jet") process to perturb molecules on a SERS active substrate to track the dynamics of the different contributions to SERS. By use of the snow jet process we are able to increase SERS signals on substrates by 500% or more while simultaneously increasing the peak:background intensity ratio. We identify components of the signal arising from changes in molecular distribution and surface morphology using a multiplexed time-varied exposure technique developed in-house. This allows us to distinguish between processes decaying over time and those decaying due to laser heating. Our study goes a long way toward disentangling the different contributions to SERS peak and background continuum signals and points to the different origins of these two co-occurring processes on nanostructured plasmonic substrates. This deeper understanding of the SERS process is crucial to allow SERS to reach its full potential.

1. INTRODUCTION

Surface-enhanced Raman scattering (SERS) remains a highly active research area, but despite the commercial availability of SERS substrates, the technique has yet to gain widespread commercial or industrial adoption. The true complexity in understanding SERS spectra hinders its acceptance in the broad spectroscopy community, with the difficulty in obtaining reliable quantitative information from SERS spectra being a key issue. The origins of SERS have been much debated since its discovery in the 1970s.[1−3] The principal amplification of SERS is caused by the electromagnetic (EM) field enhancement from plasmonic nanostructures with enhancement factors between 10^4 and 10^{14} frequently quoted in the literature.[4,5] This enhancement can be optimized by tuning plasmons into resonance with the input laser excitation and the outgoing Raman scattered wavelengths.[6,7] Accompanying the EM enhancement is an enhancement due to the surface chemistry, the chemical enhancement (CE). The CE is generally far less than the EM enhancement, but the CE is strongly system dependent, varying with applied potential and wavelength, and in certain charge-transfer systems it can dominate over the EM enhancement.[8] In experimental SERS spectra, therefore, it is difficult to precisely distinguish between the EM and CE nature of the enhancement and most current work focuses on the larger EM enhancement.

As well as the complex EM and CE enhancements, SERS signals are accompanied by an underlying broad continuum, the "background". The background has proved to be one of the most enduring elements of SERS remaining to be understood. It has received relatively little attention in recent years by the SERS community, with many ignoring it completely. It is generally assumed to occur due to the coupling between the well-defined energy levels in the molecular system and the broad electronic continuum of energy states in the metal (though many groups attribute it to "surface contamination"). There are many competing theories as to the exact mechanism causing this background, most of which emerged toward the end of the 1970s[9−13] and have been reviewed by Furtak and Reyes.[14] A more promising model based on coupling between the molecule and its image dipole in the metal substrate has recently been discussed and developed by our group.[15] On top of this limited progress, none of the models have attempted to predict how the background differs with substrate geometry and therefore none have been successful at accurately emulating real SERS spectra. Understanding the real nature of the background and how to control it is critical to extending SERS

to quantitative analysis and providing further enhanced signals for advanced diagnostic and analytical applications.

In this paper, well-defined plasmonic nanostructures coated with self-assembled monolayers (SAMs) of thiols are investigated. There are many factors which affect the measured SERS enhancement; the most important of these depends on the localized plasmonic resonances on the structure. Our nanostructures have localized plasmon resonances tethered to specific positions within the structure defined by its geometry.[16,17] The plasmonic areas give the principal EM part of the SERS enhancement to molecules adsorbed in those regions. In addition to this, the metal surface roughness, at atomic and greater length scales, has been shown to alter the CE effect[18−20] as well as aiding coupling of light into the plasmonic modes. The orientation of molecules on the surface affects their Raman selection rules and therefore the relative peak intensity since the Raman polarizability tensor is modified. Laser heating of the sample has also been shown to affect molecular orientation and the Raman polarizability tensor.[21]

Here we use a low-energy mechanochemical process (conventionally termed a "snow jet" process) to perturb molecules on a SERS substrate and track the dynamics of the different contributions to the SERS enhancement. This allows identification of components which arise from changes in molecular distribution and from surface morphology.

The snow jet process (depicted in Figure 1) is a commonly used cleaning procedure in nanofabrication, which removes
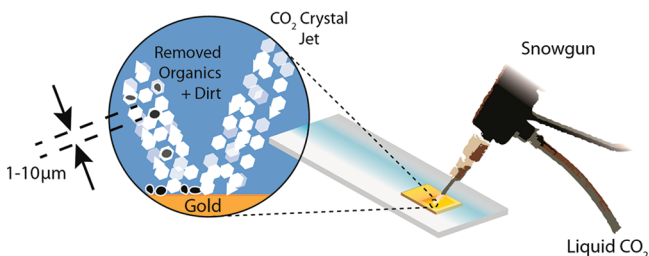

Figure 1. The snow jet process removes dirt and organic materials from the gold surface via blasting with a stream of carbon dioxide microcrystals.

organics and particulates from a surface by firing CO_2 microcrystals at it. A combination of the excellent solvent properties of CO_2, its low temperature and the momentum imparted by the crystals facilitates the cleaning.[22] Until now, the process has been used purely as a cleaning technique, principally on flat silicon surfaces where it has widespread industrial use in the silicon electronics industry. Here, we extend and study its use for cleaning nanostructured SERS substrates and as a tool for inducing transient perturbations to the SERS process allowing us to track short-term changes to the strength of the SERS signal and background. Furthermore, during SERS measurements both temporary and permanent changes to the system can occur due to the laser irradiation involved. This can cause transient changes to the substrate from local heating, annealing, changes in molecular orientation, photodamage to the molecules, or their desorption from the surface.

In this paper we study the effect of snow jet on the transient response of the SERS peaks and the background. We devise a new procedure, multiplexed time-varied exposure (MTVE), to study the time and laser heating effects on SERS. The study of the decay of snow-jet-induced transient processes coupled with

the MTVE measurements helps to distinguish the effects of laser heating from those which are a function of time (such as relaxation processes) on the SERS substrate. By use of this we disentangle the contributions to the peak and accompanying background in the SERS process. Our work points to differing origins of the peak and background signals in SERS and highlights the additional dependence of the SERS background on the local morphology. Our study goes a long way to deepen the understanding of the SERS process and the accompanying SERS background.

2. EXPERIMENTAL SECTION

2.1. Substrate Preparation. The SERS substrates used were Klarite (Renishaw Diagnostics Ltd., Glasgow, UK, formerly D3 Technologies). Klarite is a commercially available gold-coated inverted pyramid structure with plasmon resonances tuned to give optimal SERS enhancement at 785 nm laser radiation, a commonly used Raman excitation wavelength. SAMs of benzenethiol (BTh) were formed on Klarite by placing the new, clean substrates into 10 mM ethanolic solution for at least a few hours before being removed and washed thoroughly with ethanol to remove any excess thiol. This is a well-documented technique for forming SAMs.[23]

2.2. Snow Jet Experiments. The samples were snow jetted with solid carbon dioxide crystals using a snow jet unit manufactured by Applied Surface Technologies. The samples (mounted on a microscope slide) were vacuum clamped to a hot plate, with the sample surface reaching a temperature of $T = 100$ °C just prior to snow jetting to reduce ice build-up during the process. This momentary uniform heating causes a small decrease in the average SERS peak intensities. As described later, this further supports the conclusions drawn in this study that despite this decrease, snow jetting results in massive improvements in signal. The samples were snow jetted for a period of 2 min with the jet continuously moving around the active area of the sample.

2.3. Raman Measurements. An SE1000 (Renishaw Diagnostics Ltd.) desktop Raman system equipped with a 185-mW 785-nm laser was used for the SERS measurements. Raman spectra were taken with 10 s integration times and 2 acquisitions. The laser has a large spot-size of 120 μm. The average power density in this case is 1.6 kW/cm^2, which is at least a few orders of magnitude less than those typically used in SERS measurements (∼MW/cm^2). Most importantly, there was no significant evidence in the SERS spectra of laser damage to the thiol when compared to control experiments with a more focused laser which resulted in burning and decomposition of the thiol as indicated by a reduction of the thiol peaks' intensities and the growth of a peak at 980 cm^{-1} corresponding to the oxidation of the sulfur headgroup[24] (data not shown). To further minimize the impact of any desorption effect, the points were pre-exposed to the laser illumination to energetically remove any loosely bound thiols, which reduced the signal to a stable point before MTVE measurements were made. In-house software was developed in Igor Pro (Wavemetrics Inc.) to control the instrument and record spectra in array and time-resolved SERS measurements. The MTVE technique was used to distinguish between time-dependent and laser heating dependent relaxation processes and is explained in detail below.

2.4. Multiplexed Time-Varied Exposure Raman Measurements. To help distinguish between effects caused by heating under laser illumination and those that are dependent on time, we developed the MTVE technique illustrated in parts
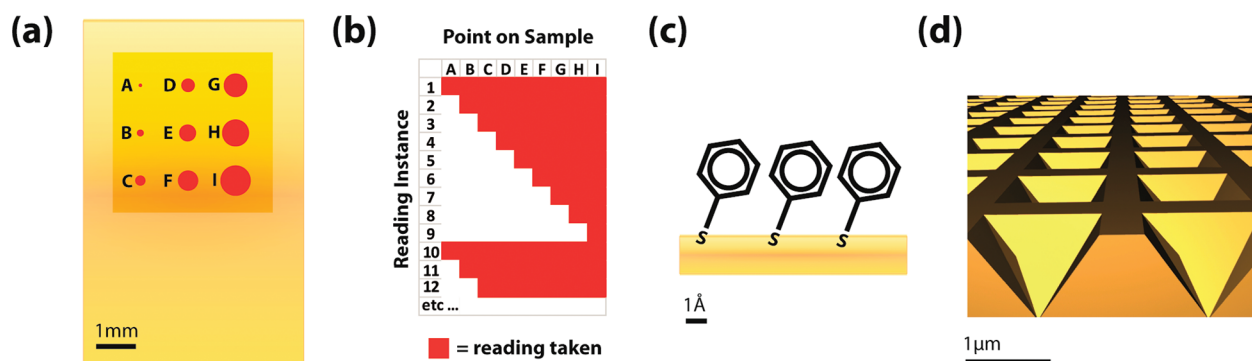
Figure 2. (a) Exposure regions on Klarite nanostructured area (4 mm × 4 mm) with size of dot indicating relative total exposure time over course of experiment. (b) Table showing exposure sequence of the different points as per the MTVE process. (c) Schematic showing the attachment of a BTh monolayer on a gold surface. (d) Klarite nanostructure 3D cross-section showing square-array of inverted pyramids (1.5 μm × 1.5 μm).

a and b of Figure 2. In this technique an array of nine well-spaced points is chosen on the Klarite sample. The array is scanned using a computer-controlled XY translation stage. The sample (mounted on a microscope slide) was locked into position using the built-in sample clamp on the stage to ensure the same points were measured before and after snow jetting. The points illuminated may differ slightly due to stage repeatability; however we believe any effect of this to be minimal due to the large spot-size. A Raman spectrum is recorded at each point in the array with a 10 s integration time (two acquisitions). This forms the first reading. After a period of time (T = 15 min here) a further set of measurements of the point array is taken, this time at every point in the array except one (in this case, point A). Over these two sets of readings, point A therefore has had less total exposure to the laser compared to all the other points. On subsequent measurement sets, one less point is measured each time, until only one point in the array (point I) is measured (this happens on the ninth measurement set here). On the next measurement set, the whole process repeats and all the points are measured again. This procedure continues until the end of the experiment. This results in data from an array of points on the sample which have had varied amounts of exposure to the laser, but have been measured regularly over the total time period (on the order of days). This means point H has been exposed 89% of the time point I was (which was exposed every time), point G was exposed 78% of the time point I was, and so forth.

The MTVE technique was performed both before and after the sample had been snow jetted to observe the transient behavior of the SERS signals over a day or so.

2.5. Raman Mapping Measurements. Raman mapping measurements were performed using an inVia microscope (Renishaw plc., Wotton-under-Edge, UK) using a 5× objective. A Klarite sample was coated with a BTh SAM as previously described. A Raman map was recorded over a large area of the sample (0.4 mm × 4 mm) using a 785 nm line laser and the streamline acquisition mode (WiRE 3.3). The laser power was reduced to such an extent as to not alter the signal of BTh on repeated measurements of the same area. The total acquisition time was 1 h, and 4247 spectral points were recorded. A restricted area of the sample was then snow jetted for 2 min (as in MTVE experiments) and a comparative Raman map was recorded afterward of the same area.

3. RESULTS AND DISCUSSION

3.1. Removal of Non-thiol Organics. A Klarite sample coated with a benzenethiol SAM was left in ambient atmosphere over a period of a few days, during which time it becomes weakly contaminated with other organics as identified in the SERS spectra in Figure 3. After the sample was snow
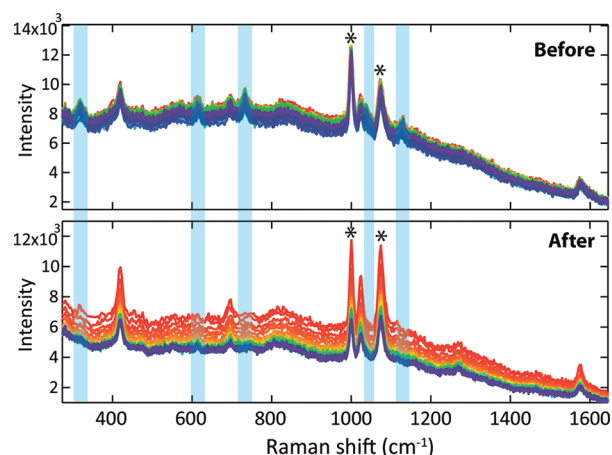

Figure 3. Fingerprint region of the SERS spectra of a BTh monolayer on Klarite before (top) and after (bottom) snow jetting (with time progressing from red to blue spectra). Presence of non-BTh peaks (before snow jetting) indicated with blue shaded boxes. Distinct changes to relative peak heights are highlighted with an asterisk.

jetted the non-BTh peaks disappear from the SERS spectra indicating removal of organics which had been adsorbed into the BTh SAM. The contaminants, with low bonding affinity to gold, are removed by dissolution in the CO_2 crystals impinging on the surface and bouncing off, while the BTh, with its high bonding affinity to gold, remains attached to the surface. The snow jet process is thus able to clean the surface of unwanted organics while leaving target molecules unharmed, which supports existing studies that show the snow jet process can remove non-bound organics as well as dirt.[25,26] Figure 3 also shows evidence of new SERS peaks appearing at 1269 and 1460 cm^{-1} after snow jetting. These modes can be assigned to the 3(b_2) bending and 19b(b_2) stretching lines of BTh and indicate a reorientation of the BTh molecules on the surface, since, based on the Raman selection rules, these modes should be enhanced for molecules lying flatter on the surface.[27−29]

In Figure 3 we also observe relative peak intensity changes between the spectra before and after snow jetting. This is especially evident in the benzene ring modes between 999 and 1074 cm^{-1}. The ratio of the 999/1074 cm^{-1} peaks changes from 0.6 before snow jetting to 1.1 after snow jetting. This clearly indicates a change in the BTh polarizability tensor and is suggestive of a reorientation or phase-change of the SAM. Over the course of the experiment, this relative peak height *did not* revert to its original position but remained constant, indicating a permanent change, and is therefore not linked to the subsequent decay in SERS signals. This reorientation could be linked to the removal of nonbound organics, as these do not return over the time scales explored here as evidenced by the lack of reappearance of non-BTh peaks in the post-snow jet SERS spectra.

3.2. SERS Peak and Background Signal Before and After Snow Jet.

3.2.1. MTVE. The peak height (defined as the absolute intensity minus the background) of the different vibrational modes of BTh is the same for all measurement points before snow jetting (within a variation of <15%). The peak height for the 1074 cm^{-1} BTh ring-breathing mode is plotted in Figure 4.
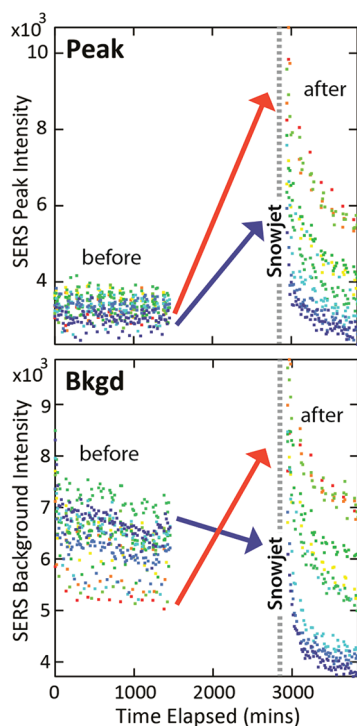

Figure 4. 1074 cm^{-1} BTh peak intensity only (top) and the background intensity (bottom) before and after snow jetting. Points on sample represented by color from the least measured point A (red) to most measured point I (dark blue).

Background heights (taken from a spectral position near each peak) before snow jetting vary slightly more in absolute intensity (±20% of mean) for the different sample points and unlike the peak height drop off over initial MTVE measurements before snow jetting (by around 5%). This indicates that the background is much more sensitive than the peak to the surface environment and spectral acquisition conditions.

After snow jetting, the intensity of the 1074 cm^{-1} BTh SERS peak increased across all points on the sample but by differing amounts depending on the measurement point. This was

similar for all the other BTh peaks (not shown). In contrast the background intensity after snow jetting either increased or decreased depending on the position on the sample. This was also consistent for all other positions on the background. That the increase in peak intensity is not always accompanied by an increase in background intensity clearly indicates that the two are decoupled from each other and suggests different origins to the signal change.

3.2.2. Raman Map. The Raman maps of the Klarite sample before and after snow jetting support the data obtained via the MTVE experiments. The areas of the sample that had not experienced the snow jet showed a slight decrease in the average peak intensities (see Experimental section 2.2) while the snow jetted area displays a clear enhancement over the non-snow jetted areas of the sample as shown in Figure 5. The snow jetted area produced an enhancement of benzenethiol peaks up to 15 times.
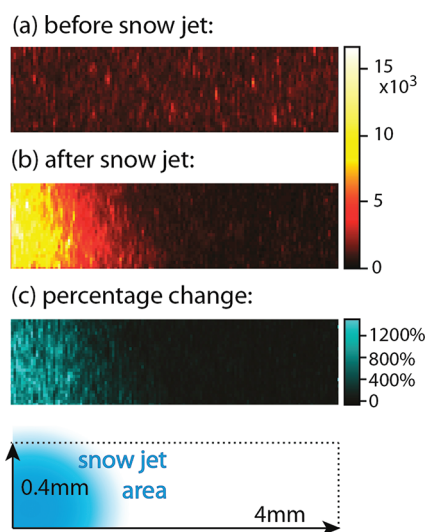

Figure 5. Integrated intensity maps of the 999-cm^{-1} BTh ring-mode peak (a) before and (b) after snow jetting a restricted area of the sample as indicated in the diagram. Percentage increase in integrated intensity after snow jetting is shown in (c). The increase in the snow jetted area is up to >1500%.

3.3. Signal Decay after Snow Jetting Using MTVE.

After snow jetting, both the SERS peak and background signal begin to decay away from their new levels as seen in Figures 4 and 6. The decay occurs both as a function of exposure (presumably via laser heating) and as a function of time elapsed after snow jetting. The peak signal drops back to its original level after snow jetting, suggesting that the number of thiol molecules attached to the surface has not changed significantly and that they return to a similar state to that before snow jetting. The background signal also decays but not necessarily back to the position it started at before snow jetting. By use of the MTVE method discussed above, we can gain insight into the dominant processes causing these decays. Figure 6a shows the decay of the 1074 cm^{-1} BTh breathing mode (other peaks follow similar decay trends) and parts b and c show a nearby background point not associated with any vibration mode of the molecule (1107 cm^{-1}) plotted against both the number of measurements made (proportional to laser exposure time on the sample) and real time expired. The intensity has been normalized to the initial measurements of each point, to allow
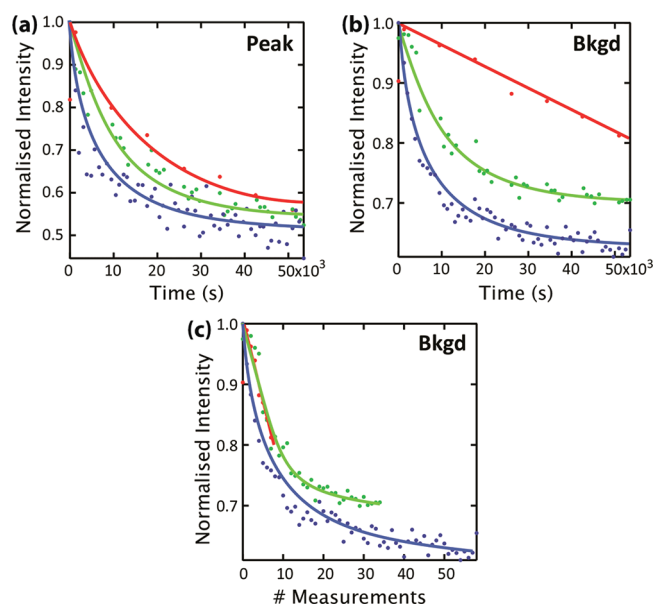
Figure 6. (a) SERS peak height of the BTh ring-breathing mode at 1074 cm^{-1} (background subtracted using the intensity at 1107 cm^{-1}) vs total time elapsed. (b) Intensity of the SERS background at 1107 cm^{-1} vs total time elapsed and (c) vs number of measurements taken. Three different MTVE sample points are shown. Traces colored as in Figure 4 with red (point A, least measured), green (point E, midnumber of measurements), and blue (point I, most measured). All lines are guides to the eye.

better comparison of trace shapes. It is immediately evident that the peak height and background signals decay at different rates, with the background especially affected by the number of measurements. Comparing decay shapes shows that the peak height decay process is principally dependent on real time expired, whereas the background signal has a more significant component related to the number of measurements taken. This reinforces the differing origins of changes to the background and peak signals, both of which are modified by the snow jet: one decays principally over time, while the other decays also as a function of laser exposure.

To identify the natural decay of the system irrespective of measurement artifacts, we fit an exponential to the intensity vs time decays of the SERS peak and background signals. Because of the mixed nature of the decay, exponentials will not provide a precise decay profile, but they satisfactorily track the relative total decay times. Plotting these decay times as a function of fractional measurement frequency (where the maximum frequency of 1.0 corresponds to Point I which is measured every time, and 0.0 corresponds to a hypothetical point which cannot be measured) and extrapolating gives an estimate for the natural decay time of the system *without* laser measurement (Figure 7). This shows that the natural (non-heat related) decay time is around 7.0 h for the peak signal and 9.3 h for the background signal.

3.4. Discussion and Analysis. Snow jetting the SERS active substrate, as well as removing loosely bound hydrocarbons from the surface significantly boosts the SERS signal obtained from the strongly bound thiol by on average 250% for the 1074 cm^{-1} line across the entire sample (Figure 4). This is similar (or even more) for all the other SERS peaks (not shown), with enhancements of up to 500% found for certain peaks and regions.
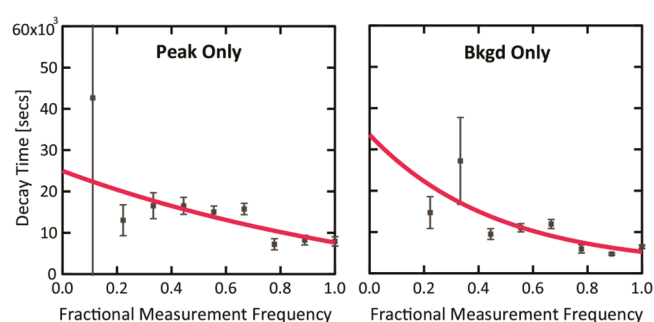

Figure 7. Extracted decay times for all points plotted against fractional measurement frequency (defined in text). The *y*-axis intercept of the extrapolated fit provides an estimate for the decay time of a hypothetical non-measured point on the sample.

The action of snow jetting affects the SERS peak of the molecule and the background signal in dissimilar ways pointing to the different origins of these processes. The molecular SERS peak signal is always boosted in intensity after snow jetting, before decaying away over time (>12 h) toward its original value. However the background signal intensity varies differently depending on position on the sample with some points showing an increase after snow jet and some showing a decrease. Irrespective of the level of background signal after snow jet, the signal then decays, with a key component due to laser exposure, and does not return to its original level, unlike the peak signal.

The snow jet process imparts momentum locally to the Klarite surface and the organics held on it, and this can cause the molecules to change orientation and position over very small scales. One proposal is that molecules are pushed deeper into nanocrevices that exist between the gold clusters formed during the evaporation process (as depicted in Figures 8 and 9).
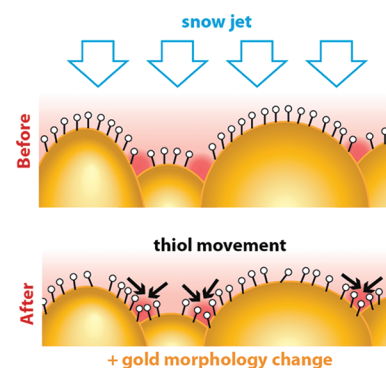

Figure 8. BTh molecules (not to scale) on an evaporated gold surface showing location of nanocrevices with enhanced EM fields before and after snow jetting. BTh molecules are pushed into the crevices by the snow jet process and also reorient. The gold surface itself is also modified by the snow jet process.

Since the radii of curvature of these nanocrevices is much smaller than the wavelength of light, we expect localized field enhancements in these regions as previously identified and modeled in nanoscale grating grooves and crevices between nanoscale silver cylinders.[30,31] The work of Van Duyne and co-workers also highlight the significance of surface roughness to the SERS enhancement in their work on metal film over silica nanosphere (MFON) surfaces.[32,33] Molecular diffusion of thiols is well-known on gold surfaces;[34,35] hence we propose
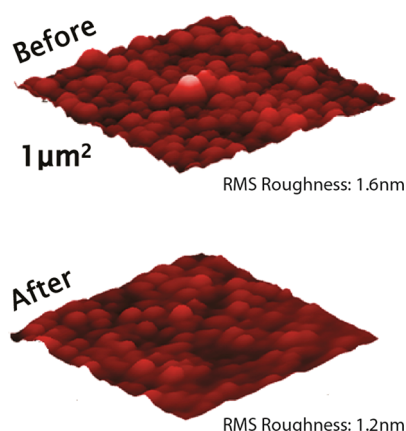
Figure 9. Atomic force microscopy scans of the gold Klarite surface before and after snow jetting, showing 25% reduction in rms roughness after snow jetting.

that the SERS peak signals rise transiently due to concentration of molecules in these nanocrevices, and then over time the molecules diffuse across the surface back to their original lower energy configuration, with the signal returning to its initial value as a consequence. Such 2D molecular migration has not so far been tracked in real time as here, and gives new insight into their motion on the nanoscale, and how this can be externally affected.

Along with molecules being pushed into nanocrevices, molecular reorientation takes place as evident by changes in the SERS peak intensity ratios. Much slower decays of the peak intensity are due to slight air-mediated degradation of the SAM over time as evidenced by the re-emergence of the 614 cm^{-1} peak after snow jetting corresponding to an S=O stretching mode. We do not, however, see the peak at 980 cm^{-1} attributed to oxidation observed during our control laser heating experiments (see Experimental section 2.3) and postulate that this could be due to differences in oxidation state of the thiol group in the two cases.

Background signals are also enhanced by high local electric fields.[15,36] Hence the instantaneous changes in the background are also related to the concentration effect of snow jet moving molecules into nanocrevices. To explain the longer term effects we note that the background is much more sensitive to nanoscale surface geometry than the SERS peaks. This is seen in the different relative SERS:background contributions from nanoparticle vs nanostructured surfaces and from the greater variability of the background at different locations on such samples. We thus believe that the snow jet process produces nanoscale changes to the gold structure, morphology, or roughness, which causes changes in the background signal that either increases or decreases depending on the competitive effects of local enhancement and surface roughness. Atomic force microscopy measurements before and after snow jetting indicate a slight large-scale smoothing of the surface, with the root-mean-square (rms) roughness being reduced by 25% as shown in Figure 9. This appears to have both permanent (as the background does not return to its original value) and transient effects (since the background does decay after snow jetting). Since the background signal is linked with molecular locations, as observation of the background requires molecules,[15] one component of the dynamics should follow that of the peak, which is indeed observed. In addition, the background signal decays as a function of laser exposure. We

suggest that the laser causes local heating of the sample which can affect the fine structure of gold via an accelerated annealing process. The SERS peaks are not significantly affected by the number of measurements (laser heating) and have a decay pathway (after snow jet perturbation) as proposed by the model in Figure 8; however, in contrast, the background depends on local morphology and surface roughness and hence, its decay is dependent on annealing processes, which are likely to be accelerated by laser heating.

4. CONCLUSION

Understanding the background is essential to establish SERS as a mainstream technique for developing quantitative applications. This study highlights the different origins of the SERS background compared to those of the SERS peak signal. By use of a soft mechanochemical process to perturb the surface of a standard SERS substrate we subsequently track changes to the peak and background as a result of heating and time using a newly developed MTVE technique. This allows us to identify the different contributions to the peak and background signals with differing decay channels. The background is shown to be highly dependent on gold morphological changes unlike the peak. This allows us to identify the possibility of reducing the SERS background signal at the same time as increasing the SERS peak signal, desirable for many applications. The results obtained cannot entirely be explained by current SERS theories and thus highlight the need for more in-depth studies of the SERS background based on the geometry of SERS substrates. This work paves the way for new studies into the SERS background and new methods for temporarily perturbing SERS substrates to increase the peak to background signal-to-noise.

■ AUTHOR INFORMATION

Corresponding Author
*E-mail: sm735@cam.ac.uk (S.M.); jjb12@cam.ac.uk (J.J.B.).

Notes
The authors declare no competing financial interest.

■ REFERENCES

(1) Fleischmann, M.; Hendra, P. J.; McQuillan, A. J. *Chem. Phys. Lett.* **1974**, *26*, 163−166.
(2) Jeanmaire, D. L.; Van Duyne, R. P. *J. Electroanal. Chem. Interfacial Electrochem.* **1977**, *84*, 1−20.
(3) Albrecht, M. G.; Creighton, J. A. *J. Am. Chem. Soc.* **1977**, *99*, 5215−5217.
(4) Kneipp, K.; Wang, Y.; Kneipp, H.; Perelman, L. T.; Itzkan, I.; Dasari, R. R.; Feld, M. S. *Phys. Rev. Lett.* **1997**, *78*, 1667.
(5) Nie, S.; Emory, S. R. *Science* **1997**, *275*, 1102−1106.
(6) Mahajan, S.; Abdelsalam, M.; Suguwara, Y.; Cintra, S.; Russell, A.; Baumberg, J.; Bartlett, P. *Phys. Chem. Chem. Phys.* **2007**, *9*, 104−9.
(7) Haynes, C. L.; Van Duyne, R. P. *J. Phys. Chem. B* **2003**, *107*, 7426−7433.
(8) Uetsuki, K.; Verma, P.; Yano, T.-a.; Saito, Y.; Ichimura, T.; Kawata, S. *J. Phys. Chem. C* **2010**, *114*, 7515−7520.
(9) Otto, A.; Timper, J.; Billmann, J.; Kovacs, G.; Pockrand, I. *Surf. Sci.* **1980**, *92*, L55−L57.

(10) Heritage, J.; Bergman, J.; Pinczuk, A.; Worlock, J. *Chem. Phys. Lett.* **1979**, *67*, 229−232.

(11) Otto, A. *Surf. Sci.* **1980**, *92*, 145−152.

(12) Burstein, E. *Solid State Commun.* **1979**, *29*, 567−570.

(13) Gersten, J.; Birke, R.; Lombardi, J. *Phys. Rev. Lett.* **1979**, *43*, 147−150.

(14) Furtak, T. E.; Reyes, J. *Surf. Sci.* **1980**, *93*, 351−382.

(15) Mahajan, S.; Cole, R. M.; Speed, J. D.; Pelfrey, S. H.; Russell, A. E.; Bartlett, P. N.; Barnett, S. M.; Baumberg, J. J. *J. Phys. Chem. C* **2010**, *114*, 7242−7250.

(16) Perney, N. M. B.; Abajo, F. J. G.; de; Baumberg, J. J.; Tang, A.; Netti, M. C.; Charlton, M. D. B.; Zoorob, M. E. *Phys. Rev. B* **2007**, *76*, 35425−35426.

(17) Kelf, T. A.; Sugawara, Y.; Cole, R. M.; Baumberg, J. J.; Abdelsalam, M. E.; Cintra, S.; Mahajan, S.; Russell, A. E.; Bartlett, P. N. *Phys. Rev. B* **2006**, *74*, 12.

(18) Saito, Y.; Wang, J. J.; Smith, D. A.; Batchelder, D. N. *Langmuir* **2002**, *18*, 2959−2961.

(19) Doering, W. E.; Nie, S. *J. Phys. Chem. B* **2002**, *106*, 311−317.

(20) Otto, A.; Mrozek, I.; Grabhorn, H.; Akemann, W. *J. Phys.: Condens. Matter* **1992**, *4*, 1143−1212.

(21) Moskovits, M.; DiLella, D. P.; Maynard, K. J. *Langmuir* **1988**, *4*, 67−76.

(22) Sherman, R.; Hirt, D.; Vane, R. *J. Vac. Sci. Technol., A* **1994**, *12*, 1876.

(23) Love, J. C.; Estroff, L. A.; Kriebel, J. K.; Nuzzo, R. G.; Whitesides, G. M. *Chem. Rev.* **2005**, *105*, 1103−69.

(24) Schoenfisch, M. H.; Pemberton, J. E. *J. Am. Chem. Soc.* **1998**, *120*, 4502−4513.

(25) Sherman, R. *J. Vac. Sci. Technol., B* **1990**, *8*, 563.

(26) Sherman, R. *J. Vac. Sci. Technol., B* **1991**, *9*, 1970.

(27) Socrates, G. *Infrared and Raman characteristic group frequencies: tables and charts*; 3rd ed.; Wiley: 2004.

(28) Joo, T. H.; Kim, M. S.; Kim, K. *J. Raman. Spectrosc.* **1987**, *18*, 57−60.

(29) Lombardi, J. R.; Birke, R. L. *J. Phys. Chem. C* **2008**, *112*, 5605−5617.

(30) Sobnack, M.; Tan, W.; Wanstall, N.; Preist, T.; Sambles, J. *Phys. Rev. Lett.* **1998**, *80*, 5667−5670.

(31) García-Vidal, F.; Pendry, J. *Phys. Rev. Lett.* **1996**, *77*, 1163−1166.

(32) Litorja, M.; Haynes, C. L.; Haes, A. J.; Jensen, T. R.; Van Duyne, R. P. *J. Phys. Chem. B* **2001**, *105*, 6907−6915.

(33) Dick, L. A.; McFarland, A. D.; Haynes, C. L.; Duyne, R. P. Van *J. Phys. Chem. B* **2002**, *106*, 853−860.

(34) Barrena, E.; Ocal, C.; Salmeron, M. *J. Chem. Phys.* **1999**, *111*, 9797.

(35) McCarley, R. L.; Dunaway, D. J.; Willicut, R. J. *Langmuir* **1993**, *9*, 2775−2777.

(36) Farcau, C.; Astilean, S. *Chem. Commun.* **2011**, *47*, 3861−3.